



# A detailed spectroscopic analysis of the growth of oxy-carbon species on the surface of Pt/Al<sub>2</sub>O<sub>3</sub> during propane oxidation



Casey P. O'Brien, Ivan C. Lee \*

U.S. Army Research Laboratory, Sensors and Electron Devices Directorate, 2800 Powder Mill Road, Adelphi, MD 20783, USA

## ARTICLE INFO

## Article history:

Received 3 March 2016

Revised 2 November 2016

Accepted 28 December 2016

Available online 21 January 2017

## Keywords:

Propane oxidation

Platinum

Carbon

Spectroscopy

## ABSTRACT

The growth of oxygenated carbonaceous (oxy-carbon) species on the surface of Pt/Al<sub>2</sub>O<sub>3</sub> during total oxidation of propane is analyzed in detail—including their composition, their location on the catalyst surface, their reactivity, and their role in the propane oxidation mechanism—by *in situ* diffuse reflectance infrared Fourier-transform spectroscopy (DRIFTS). Platinum nanoparticles catalyze the transformation of propane into many different oxy-carbon surface species, including acetate, enolate, aliphatic ester, and acetone, which spillover and grow on the Al<sub>2</sub>O<sub>3</sub> support. There is no correlation between the concentration of oxy-carbon surface species and the rate of CO<sub>2</sub> production in the gas-phase, which indicates that these species are inert spectators in the propane oxidation mechanism. Temperature-programmed oxidation of the oxy-carbon surface species reveals that enolate, aliphatic ester, and acetone species are removed from the surface by combustion at similar temperatures with an activation barrier of 112 kJ/mol, whereas acetate species are removed at higher temperatures with an activation barrier of 147 kJ/mol. Both the formation and combustion of oxy-carbon surface species occur in pathways that are parallel to, and orders-of-magnitude slower than, the main pathway to CO<sub>2</sub> production.

Published by Elsevier Inc.

## 1. Introduction

Heterogeneous catalysts are used for combustion of hydrocarbons in applications that require lower temperature, and greater control over the combustion process, than thermal combustion [1]. In our previous work [2], we studied the kinetics of propane combustion over Pt/Al<sub>2</sub>O<sub>3</sub> as a function of the O<sub>2</sub>/C<sub>3</sub>H<sub>8</sub> ratio in the 150–300 °C temperature range. We showed that the reaction rate was controlled to a large extent by the chemisorbed oxygen coverage on the platinum nanoparticles. However, at higher O<sub>2</sub>/C<sub>3</sub>H<sub>8</sub> ratios and lower temperatures we observed a slow deactivation of the Pt/Al<sub>2</sub>O<sub>3</sub> catalyst over hundreds of minutes that is not consistent with a slow change in the chemisorbed oxygen coverage, and must be related to deactivation of the catalyst.

There are many possible causes of the catalyst deactivation during propane oxidation, including sintering of the Pt particles, platinum-oxide formation, and the accumulation of poisoning species [3,4]. Using diffuse reflectance infrared Fourier-transform spectroscopy (DRIFTS) of adsorbed CO on the platinum nanoparticles, we observed slow formation of a specific platinum-oxide phase (PtO), which has a characteristic CO-DRIFTS band at

2123 cm<sup>-1</sup>, on the surface of the platinum nanoparticles which is likely the cause of the deactivation. The extent of PtO formation decreased with increasing temperature, and as a result, catalyst deactivation was less severe at higher temperatures. Although there was strong evidence that formation of platinum-oxides on the surface of platinum nanoparticles is at least partially responsible for deactivating the catalyst, we could not rule out the possibility that some other mechanism, such as the accumulation of poisoning species on the surface of the catalyst, could also be responsible for deactivating the catalyst.

Fourier-transform infrared (FTIR) spectroscopy is a powerful technique for elucidating the mechanisms of surface reactions, including deactivation of catalysts from accumulation of poisoning species. There have been several *in situ* FTIR studies of propane oxidation over a variety of catalysts, including Pd/CeO<sub>2</sub>/Al<sub>2</sub>O<sub>3</sub> [5], Pt/Al<sub>2</sub>O<sub>3</sub> [6–8], Pt/WO<sub>x</sub>/Al<sub>2</sub>O<sub>3</sub> [8], MgCr<sub>2</sub>O<sub>4</sub> [9,10], Co<sub>3</sub>O<sub>4</sub> [10], CuO [10], and Pt/CeO<sub>2</sub>-ZrO<sub>2</sub> [11]. Many different species have been identified on the surface of these catalysts during propane oxidation using *in situ* FTIR spectroscopy, including formate (HCOO<sup>-</sup>) [5,8–10], acetate (CH<sub>3</sub>COO<sup>-</sup>) [8–10], carbonate (CO<sub>3</sub><sup>2-</sup>) [5,7,8,11], bicarbonate (HCO<sub>3</sub><sup>-</sup>) [11], isopropoxide ((CH<sub>3</sub>)<sub>2</sub>CHO<sup>-</sup>) [10], acetone ((CH<sub>3</sub>)<sub>2</sub>CO) [9,10], and other unidentified species [6]. However, it is not clear from their results whether these species are reactive intermediates, poisoning species, or spectator species.

\* Corresponding author.

E-mail address: [ivan.c.lee2.civ@mail.mil](mailto:ivan.c.lee2.civ@mail.mil) (I.C. Lee).

The objective of this work was to characterize the growth of oxy-carbon species on the surface of Pt/Al<sub>2</sub>O<sub>3</sub> during propane oxidation in detail—including their composition, their location, their reactivity, and their role in the propane oxidation mechanism—using DRIFTS. There are many different oxy-carbon species that grow—primarily on the Al<sub>2</sub>O<sub>3</sub> support—during propane oxidation. There is no correlation between the concentration of these oxy-carbon surface species and the rate of CO<sub>2</sub> production in the gas-phase, and these species are inert spectators in the propane oxidation mechanism. Temperature-programmed oxidation (TPO) of these oxy-carbon species reveals that acetate species are less reactive than, and are removed from the surface during TPO at higher temperatures than, enolate, aliphatic ester, and acetone species.

## 2. Experimental

The catalyst preparation conditions, pre-treatment conditions, and instruments used in this work have been described in detail previously [2]. Briefly, the Pt/Al<sub>2</sub>O<sub>3</sub> catalyst was prepared by incipient wetness impregnation of  $\gamma$ -Al<sub>2</sub>O<sub>3</sub>. The as-prepared Pt/Al<sub>2</sub>O<sub>3</sub> catalyst (16.5% Pt loading) was diluted with Al<sub>2</sub>O<sub>3</sub> to give a Pt loading of 2%. The sample cup of a Praying Mantis High Temperature Reaction Chamber (Harrick Scientific Products, Inc.) was filled with approximately 25 mg of the Pt/Al<sub>2</sub>O<sub>3</sub> catalyst. The catalyst was pretreated in the reaction chamber by oxidation and reduction at 600 °C [2]. Following pre-treatment, the catalyst was heated to the reaction temperature while flowing Ar through the reaction chamber.

Propane oxidation experiments were conducted isothermally at atmospheric pressure by flowing Ar (Airgas, 99.999%), O<sub>2</sub> (Airgas, 99.999%) and a (4.0 ± 0.1%) propane in Ar balance gas mixture (Airgas) to the reaction chamber. Mass Flow controllers (MKS Instruments 1179A Mass-Flo<sup>®</sup>) were used to regulate the flow rates of gases to the high temperature reaction chamber. Two different feed gas conditions with different O<sub>2</sub>/C<sub>3</sub>H<sub>8</sub> ratios (5 and 20) were used during propane oxidation experiments, which are summarized in Table 1. Three different reaction temperatures (200 °C, 250 °C, and 300 °C) were used for each feed gas condition for a total of six different reaction conditions. Although the rate of propane oxidation is influenced to some extent by heat or mass transport under these conditions, the propane oxidation rates are not limited by mass transport and the measured rates are related to the inherent activity of the catalyst [2]. The catalyst was pre-exposed to the O<sub>2</sub> and Ar feed gases at the reaction temperature. Following 8 min of O<sub>2</sub>/Ar pre-exposure, 15.0 mL/min of the 4% propane in Ar gas mixture was introduced to the flowing feed gas along with the O<sub>2</sub> and Ar feed gases.

A Bruker Vertex 70 FTIR spectrometer equipped with a MCT detector and a Praying Mantis<sup>™</sup> Diffuse Reflectance Accessory (Harrick Scientific Products, Inc.) was used to detect surface species on Pt/Al<sub>2</sub>O<sub>3</sub> during propane oxidation. Background DRIFTS spectra were collected during the O<sub>2</sub>/Ar pre-exposure. During the propane oxidation reaction, DRIFTS measurements were repeated 240 times with 75 scans-per-spectrum and a spectral resolution of 2 cm<sup>-1</sup>. The time required to collect each spectrum was 2 min. A Gas Chromatograph (Agilent 3000A Micro GC) and a mass spectrometer

(Agilent Technologies 5973 Mass Selective Detector) were used to monitor the composition of the gas exiting the reaction chamber simultaneously with DRIFTS measurements. The GC columns were molecular sieve, Plot U, alumina, and OV-1. The specific CO<sub>2</sub> production rate (i.e. turnover frequency) was then calculated using the fraction of CO<sub>2</sub> in the product gas measured by Micro GC [2].

Following 8 h of propane oxidation at elevated temperature, the catalyst was cooled to 25 °C while flowing the propane/O<sub>2</sub>/Ar feed gas mixture, and temperature-programmed oxidation of the oxy-carbon surface species was performed by heating the catalyst from 25 °C to 600 °C at a heating rate of 25 °C/min while flowing 3 mL/min O<sub>2</sub> and 77 mL/min Ar. The concentration of CO<sub>2</sub> in the gas exiting the reactor was monitored by mass spectrometry. The method for calculating the rate of CO<sub>2</sub> evolution and the total amount of CO<sub>2</sub> evolved is described in Section S.1 of the Supporting Information. The catalyst was held at 600 °C while flowing O<sub>2</sub> and Ar for 10 min, which was longer than the amount of time required for the mass spectrometer signal associated with CO<sub>2</sub> at *m/z* = 44 to decrease to zero. CO<sub>2</sub> was the only carbon oxidation product observed during TPO. The total amount of CO<sub>2</sub> evolved during temperature-programmed oxidation was proportional to the integral DRIFTS area in the oxy-carbon surface species region (1250–1800 cm<sup>-1</sup>), which allowed for quantitative characterization of the surface carbon concentration from the integral DRIFTS area (see Section S.2. in Supporting Information).

## 3. Results and discussion

### 3.1. Characterization of surface species

The accumulation of carbonaceous deposits on Pt/Al<sub>2</sub>O<sub>3</sub> was monitored by DRIFTS over the course of 8 h of propane oxidation with six different reaction conditions in the 200–300 °C temperature range. Fig. 1(a) shows the evolution of the DRIFTS spectra in the oxy-carbon surface species region (1250–1800 cm<sup>-1</sup>) over 8 h of propane oxidation at 300 °C with O<sub>2</sub>/C<sub>3</sub>H<sub>8</sub> equal to 20. Section S.3 in the Supporting Information shows time-resolved DRIFTS spectra collected during all six reaction conditions. A precise assignment of all the bands in the oxy-carbon surface species region from comparison to the literature is difficult due to the large number of different species that have overlapping bands in this region. We assign these bands based on literature assignments of surface-bound species that are most consistent with our results. A summary of band assignments is given in Table 2 with comparisons to literature, and the structure of the oxy-carbon species is shown in Fig. 2.

The band at 1745 cm<sup>-1</sup> is likely associated with a carbonyl stretching mode of a species containing an aliphatic ester functional group [12–14], although we cannot speculate further about the identity of this species beyond the ester functionality. The shoulder at ~1680 cm<sup>-1</sup> is also likely associated with a carbonyl stretching mode, and the position of this band is consistent with the carbonyl stretching mode of acetone on Al<sub>2</sub>O<sub>3</sub> [14–17]. Several different species could contribute to the shoulder observed near ~1650 cm<sup>-1</sup>, including  $\delta$ (HOH) of molecularly adsorbed water [18–21], and  $\nu_{as}$ (OCO) of bicarbonate (HCO<sub>3</sub><sup>-</sup>) species [18,20,22–24]. The band at 1625 cm<sup>-1</sup> is consistent with the  $\nu_{as}(\text{CH}_2=\text{CH}-\text{O}^-)$  mode of enolate species, and the bands at 1400 cm<sup>-1</sup> ( $\nu_s(\text{CH}_2=\text{CHO}^-)$ ) and 1330 cm<sup>-1</sup> ( $\delta(\text{C}-\text{H})$ ) further support this assignment [17,25–34]. There are several bands in the 1560–1590 cm<sup>-1</sup> region, and also in the 1440–1470 cm<sup>-1</sup> region, which are consistent with the positions of asymmetric and symmetric stretching modes of carboxylate (COO<sup>-</sup>) groups, respectively [8,17,33–40]. Bands at ~1580 cm<sup>-1</sup> and ~1460 cm<sup>-1</sup> are most likely associated with asymmetric and symmetric stretching of

**Table 1**

Flow rates of O<sub>2</sub>, 4% propane in Ar, and Ar in the two different O<sub>2</sub>/C<sub>3</sub>H<sub>8</sub> ratios used during propane oxidation experiments.

O <sub>2</sub> /C <sub>3</sub> H <sub>8</sub> ratio	Feed gas flow rates (mL/min)			
	O <sub>2</sub>	4% propane/Ar	Ar	Total
5	3.0	15.0	62.4	80.4
20	12.0	15.0	53.4	80.4

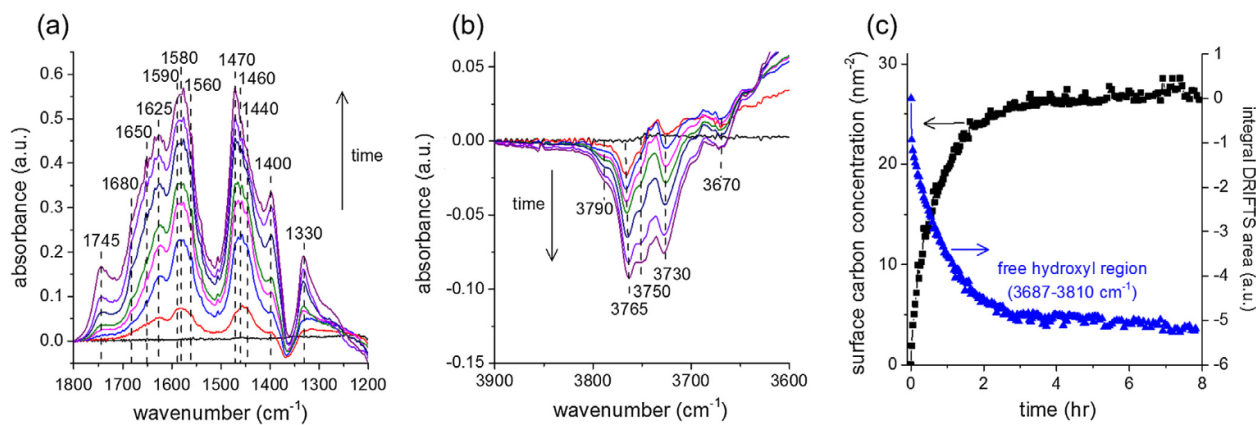


**Fig. 1.** DRIFTS spectra collected during propane oxidation over Pt/Al<sub>2</sub>O<sub>3</sub> at 300 °C and O<sub>2</sub>/C<sub>3</sub>H<sub>8</sub> equal to 20 showing the (a) oxy-carbon surface species region and the (b) O—H stretching region. (c) Surface carbon concentration (left axis, black points) and the integral area in the free hydroxyl region (3687–3810 cm<sup>-1</sup>; right axis, blue points) of DRIFTS spectra collected during propane oxidation at 300 °C with O<sub>2</sub>/C<sub>3</sub>H<sub>8</sub> equal to 20. Line colors in (a) and (b) correspond to the following propane oxidation times: black (0 min), red (1 min), blue (10 min), magenta (20 min), olive (30 min), navy (60 min), violet (120 min), and purple (470 min).

**Table 2**

Summary of the vibrational modes and positions of surface species in the oxy-carbon surface species region (1250–1800 cm<sup>-1</sup>).

Species	Vibrational mode	Band position (cm <sup>-1</sup> )	
		This work	Literature range
Acetate	v <sub>as</sub> (COO)	1580	1550–1590 [8,17–19,22,33–41]
	v <sub>s</sub> (COO)	1460	1458–1470 [8,17–19,22,33–41]
Acetone	v(C=O)	1680	1668–1725 [14–17]
	δ(CH)	1440	1434–1436 [17]
Aliphatic ester	v(C=O)	1745	1720–1753 [12–14]
Bicarbonate	v <sub>as</sub> (OCO)	1650	1646–1653 [18,20,22–24]
	v <sub>s</sub> (OCO)	1440	1438–1451 [18,20,22–24]
Enolate	v <sub>as</sub> (CH <sub>2</sub> =CH—O)	1625	1633–1655 [17,25–34]
	v <sub>s</sub> (CH <sub>2</sub> =CH—O)	1400	1392–1419 [17,25–34]
	δ(CH)	1330	1335–1338 [17,25–34]
Formate	v <sub>as</sub> (COO)	1590	1586–1597 [18,19,22,36,38–41]
Methoxy	δ <sub>as</sub> (CH <sub>3</sub> )	1470	1450–1475 [44–47]
Propionate	v <sub>as</sub> (COO)	1560	1563–1568 [42,43]
	v <sub>s</sub> (COO), δ <sub>as</sub> (CH <sub>3</sub> ), δ(CH <sub>2</sub> )	1470	1470–1475 [42,43]
Water	δ(HOH)	1650	1636–1646 [18–21]

the carboxylate group in bidentate acetate (CH<sub>3</sub>COO<sup>−</sup>) species, respectively [8,17–19,22,33–41]. The shoulder near 1590 cm<sup>-1</sup> is likely from the asymmetric stretching mode of the carboxylate group in formate (HCOO<sup>−</sup>) species [18,19,22,36,38–41]. The bands at 1560 cm<sup>-1</sup> (v<sub>as</sub>(COO<sup>−</sup>)) and 1470 cm<sup>-1</sup> (v<sub>s</sub>(COO<sup>−</sup>)) are consistent with those of the asymmetric and symmetric stretching modes,

respectively, of the carboxylate group of propionate (CH<sub>3</sub>CH<sub>2</sub>COO<sup>−</sup>) species [42,43]. Asymmetric deformation of methoxy (CH<sub>3</sub>O<sup>−</sup>) species may also contribute to the band at ~1470 cm<sup>-1</sup> [44–47]. The shoulder near 1440 cm<sup>-1</sup> is consistent with the positions of both the δ(CH) mode of acetone [16,17] and the v<sub>s</sub>(OCO) mode of bicarbonate species [18,22,24].

There are several bands observed in the 3650–3800 cm<sup>-1</sup> region of the DRIFTS spectra, shown in Fig. 1(b), which are all associated with O—H stretching vibrations of free hydroxyl groups on the Al<sub>2</sub>O<sub>3</sub> surface [24,48–50]. The assignment of these bands is based on the model of Knozinger and Ratnasamy [50]. The bands at 3790 cm<sup>-1</sup> and 3765 cm<sup>-1</sup> are associated with terminal hydroxyls attached to octahedrally-coordinated and tetrahedrally-coordinated aluminum atoms, respectively. The bands at 3750 cm<sup>-1</sup> and 3730 cm<sup>-1</sup> are associated with bridging hydroxyls that are shared by two octahedrally-coordinated aluminum atoms, and a tetrahedrally- and an octahedrally-coordinated aluminum atom, respectively. The band at 3670 cm<sup>-1</sup> is associated with hydroxyl groups attached to three octahedrally-coordinated aluminum atoms.

The intensity of the bands associated with free hydroxyls on the Al<sub>2</sub>O<sub>3</sub> surface (Fig. 1(b)) becomes more negative with increasing time, which indicates that there are hydroxyl groups on the surface of Al<sub>2</sub>O<sub>3</sub> surface at the beginning of the reaction, and these vibrational modes disappear during the reaction either by interacting with other adsorbates, or by consumption during the reaction. It is possible that hydrogen bonding between the hydroxyl groups and water or the carbonyl groups in esters or acetone decreases the concentration of free hydroxyls on the surface. Another possibility is that the hydrogen atoms in the free hydroxyl groups are displaced by the growth of oxy-carbon species on the Al<sub>2</sub>O<sub>3</sub> surface. A plot of surface carbon concentration (nm<sup>-2</sup>) versus propane

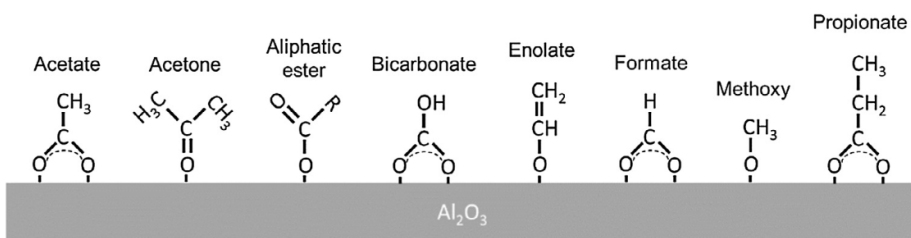


**Fig. 2.** Structures of the oxy-carbon surface species listed in Table 2, which have vibrational modes that are consistent with the band positions observed in Fig. 1(a).

oxidation time, displayed in Fig. 1(c), shows the kinetics of oxy-carbon surface species growth on Pt/Al<sub>2</sub>O<sub>3</sub> at 300 °C and with O<sub>2</sub>/C<sub>3</sub>H<sub>8</sub> equal to 20. Section S.4 in the Supporting Information shows the oxy-carbon surface species growth curves at all six reaction conditions. Also shown in Fig. 1(c) is the integral DRIFTS area in the free hydroxyl region (3687–3810 cm<sup>-1</sup>). There is a strong correlation between the growth of oxy-carbon surface species and the decay of the hydroxyl species on the surface of Al<sub>2</sub>O<sub>3</sub>. This observation suggests that oxy-carbon species grow primarily on the surface of the Al<sub>2</sub>O<sub>3</sub> support and interact with, or displace, hydroxyl groups during the growth process.

### 3.2. Temperature-programmed oxidation of oxy-carbon surface species

Temperature-programmed oxidation (TPO) of the oxy-carbon surface species was performed to quantify the amount of carbon accumulated on the surface during the reaction and to gain information about the reactivity of the oxy-carbon surface species. Fig. 3 shows the CO<sub>2</sub> evolution rates, normalized to the number of Pt sites, during TPO of the Pt/Al<sub>2</sub>O<sub>3</sub> catalyst following 8 h of propane oxidation at 300 °C with O<sub>2</sub>/C<sub>3</sub>H<sub>8</sub> equal to (a) 5 and (b) 20. The TPO profiles obtained following propane oxidation for 8 h with all six reaction conditions are shown in Section S.5 in the Supporting Information. Increasing the O<sub>2</sub>/C<sub>3</sub>H<sub>8</sub> ratio from 5 to 20 resulted in a higher total amount of CO<sub>2</sub> evolved during TPO, and a decrease in the temperature of the maximum CO<sub>2</sub> evolution rate from ~485 °C with O<sub>2</sub>/C<sub>3</sub>H<sub>8</sub> equal to 5 to ~435 °C with O<sub>2</sub>/C<sub>3</sub>H<sub>8</sub> equal to 20. In general, the total amount of CO<sub>2</sub> evolved during TPO increases, and the temperature of the maximum CO<sub>2</sub> evolution rate decreases, with increasing O<sub>2</sub>/C<sub>3</sub>H<sub>8</sub> ratio and decreasing temperature.

To understand whether all oxy-carbon species are removed from the surface at the same temperature, or whether some oxy-carbon species are more reactive than others, DRIFTS spectra were collected after removing the oxy-carbon surface species by heating in oxygen to temperatures ranging from 300 °C to 600 °C. Oxy-carbon surface species were first deposited on the surface of Pt/Al<sub>2</sub>O<sub>3</sub> by performing propane oxidation with O<sub>2</sub>/C<sub>3</sub>H<sub>8</sub> equal to 20 at 300 °C for 2 h. The catalyst was then flashed to 350 °C while flowing 3 mL/min O<sub>2</sub> and 77 mL/min Ar, and a DRIFTS spectrum was collected after cooling the sample to 300 °C. The catalyst was then flashed in a similar manner up to 400 °C, and a DRIFTS

spectrum was collected again at 300 °C. This process was repeated by increasing the flash temperature in 50 °C increments up to 600 °C. Fig. 4(a) shows the DRIFTS spectra collected after 2 h of propane oxidation, and after heating the oxy-carbon surface species in oxygen up to 350, 400, 450, 500, 550, and 600 °C.

As the flash temperature increases, the intensity of all the bands in the oxy-carbon surface species region in Fig. 4(a) decreases due to the complete oxidation of these species to CO<sub>2</sub>. However, not all of the bands decrease at the same temperature. Fig. 4(b) shows the normalized intensity of the DRIFTS bands associated with acetate (1580 cm<sup>-1</sup>), enolate (1400 cm<sup>-1</sup>), aliphatic ester (1745 cm<sup>-1</sup>), and acetone (1680 cm<sup>-1</sup>) versus flash temperature. The positions of these bands are marked in Fig. 4(a). The intensity of the bands associated with enolate, aliphatic ester, and acetone decreases at nearly identical temperatures, beginning at 350 °C until these species are completely removed from the surface after flashing the sample above 550 °C. The intensity of the band associated with acetate species, on the other hand, does not begin to decrease until 500 °C and there is still a significant amount of acetate on the surface after heating to 600 °C. These acetate species can be removed from the surface completely by holding the catalyst at 600 °C for several minutes.

The results from Fig. 4 suggest that acetate species are less reactive, and are therefore removed from the surface at higher temperatures during TPO, than the enolate, aliphatic ester, and acetone (EEA) species. It is possible that the lower reactivity of the acetate species is related to their bidentate coordination to the Al<sub>2</sub>O<sub>3</sub> surface, whereas EEA species are bound to Al<sub>2</sub>O<sub>3</sub> with only monodentate coordination. The similarity in the reaction temperature of the enolate, aliphatic ester, and acetone species may suggest that these species are interconverted to a common intermediate species which is completely oxidized to CO<sub>2</sub> in a rate-determining step.

The TPO profiles in Fig. 3 were simulated by modeling the kinetics of combustion of the lower reactivity acetate species and the higher reactivity EEA species. Power-law kinetic expressions are typically employed for modeling the kinetics of combustion of carbonaceous species on supported metal catalysts [51–54]. In addition to the power-law model, we also simulated the TPO profiles using 1st-order and 2nd-order (with respect to the surface carbon concentration) kinetic rate expressions. Details of the simulation procedure are given in Section S.6 in the Supporting Information. A detailed comparison of the simulated TPO profiles obtained with the three different kinetic models is the subject of a future publica-

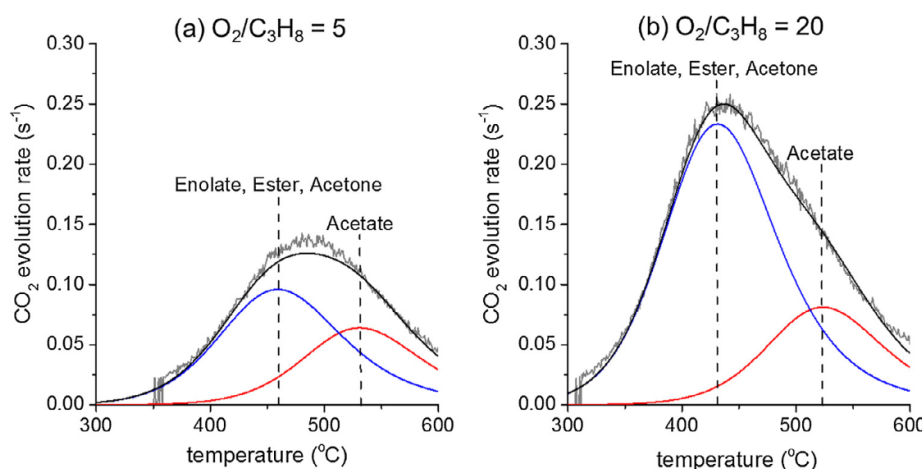


**Fig. 3.** Experimental CO<sub>2</sub> evolution rates (gray lines) during TPO of Pt/Al<sub>2</sub>O<sub>3</sub> following 8 h of propane oxidation at 300 °C with O<sub>2</sub>/C<sub>3</sub>H<sub>8</sub> equal to (a) 5 and (b) 20. The simulated CO<sub>2</sub> evolution rates (black lines) were calculated from the sum of the CO<sub>2</sub> evolution rates from combustion of acetate (red lines) and enolate, ester, and acetone species (blue lines) calculated from Eqs. (1) and (2), respectively.

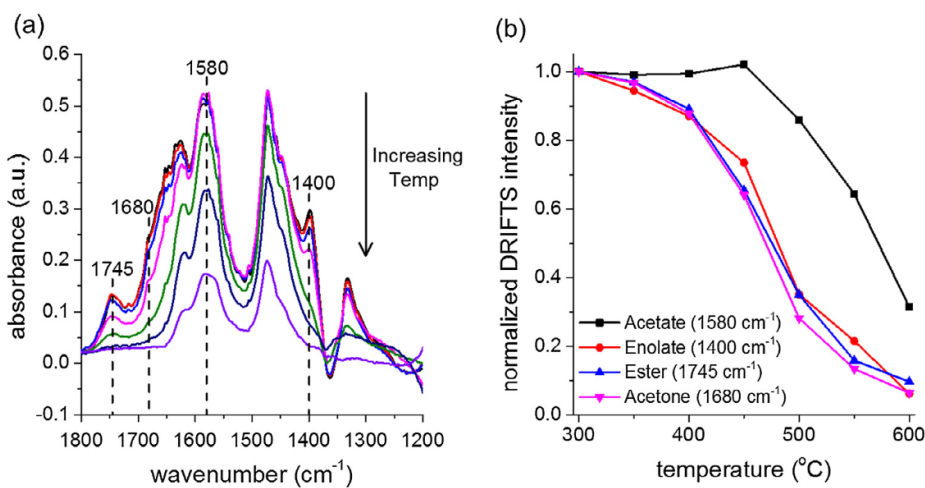


**Fig. 4.** (a) DRIFTS spectra collected after 2 h of propane oxidation with O<sub>2</sub>/C<sub>3</sub>H<sub>8</sub> equal to 20 at 300 °C (black), and after heating the catalyst in 3 mL/min O<sub>2</sub> and 77 mL/min Ar up to 350 °C (red), 400 °C (blue), 450 °C (magenta), 500 °C (olive), 550 °C (navy), and 600 °C (violet). Each spectrum was collected at 300 °C. (b) Normalized DRIFTS intensity of acetate (1580 cm<sup>-1</sup>), enolate (1400 cm<sup>-1</sup>), aliphatic ester (1745 cm<sup>-1</sup>), and acetone (1680 cm<sup>-1</sup>) species versus temperature of oxidative heat treatment.

tion. Briefly, the simulated TPO profiles from the power-law model were the best-fit to the experimental TPO profiles ( $R^2 = 0.9926$ ) due to the largest number of adjustable parameters (9). The 2nd-order model ( $R^2 = 0.9920$ ) was nearly as good of a fit as the power-law model, but with 2 fewer adjustable parameters (7). The 1st-order model, which also has 7 adjustable parameters, was the poorest fit to the experimental data ( $R^2 = 0.9853$ ).

We believe that the 2nd-order model most accurately simulates the TPO of oxy-carbon species because it fits the experimental data nearly as well as the power-law model with fewer adjustable parameters, and there is a mechanistic basis for the 2nd-order model. Fig. 3 shows the simulated TPO profiles and the CO<sub>2</sub> evolution rates from combustion of acetate and EEA species following propane oxidation at 300 °C with O<sub>2</sub>/C<sub>3</sub>H<sub>8</sub> equal to (a) 5 and (b) 20, calculated using the 2nd-order rate expressions shown in Eqs. (1) and (2), respectively,

$$r_{CO_2,Ac} = (1.8 \cdot 10^6 \text{ s}^{-1}) \cdot \exp\left(\frac{-147 \text{ kJ}}{RT}\right) \cdot [C_{Ac}]^2 \quad (1)$$

$$r_{CO_2,EEA} = (2.7 \cdot 10^4 \text{ s}^{-1}) \cdot \exp\left(\frac{-112 \text{ kJ}}{RT}\right) \cdot [C_{EEA}]^2 \quad (2)$$

where  $r_{CO_2,Ac}$  and  $r_{CO_2,EEA}$  represent the rates of CO<sub>2</sub> production (s<sup>-1</sup>) from combustion of acetate and EEA species, respectively,  $R$  represents the gas constant (J/mol/K),  $T$  represents the temperature (K), and  $[C_{Ac}]$  and  $[C_{EEA}]$  represent the concentrations (per-Pt-site) of acetate and EEA species, respectively. The simulated TPO profiles in Fig. 3 match the experimental TPO profiles well.

A comparison of the activation barriers for combustion of EEA species and acetate species from this work to those previously reported in the literature is not straightforward because the kinetics of combustion of carbonaceous deposits depends on many factors, including the composition of the carbonaceous deposits, the catalyst, and the kinetic model used to analyze the kinetics. However, the activation barrier for combustion of EEA species (112 kJ/mol) from this work is similar to that previously reported for combustion of coke on a naphtha reforming Pt/Re-Al<sub>2</sub>O<sub>3</sub> catalyst (107 kJ/mol) [55], and the activation barrier for combustion of acetate species (147 kJ/mol) from this work is in the range of values previously reported for non-catalytic combustion of carbon (130–168 kJ/mol) [56].

The concentration of acetate species on the Al<sub>2</sub>O<sub>3</sub> surface after 8 h of propane oxidation at 300 °C, which is proportional to the area of the acetate TPO curves in Fig. 3, increases slightly from ~21 per-Pt-site with O<sub>2</sub>/C<sub>3</sub>H<sub>8</sub> equal to 5, to ~27 per-Pt-site with O<sub>2</sub>/C<sub>3</sub>H<sub>8</sub> equal to 20. The concentration of EEA species is much more sensitive to the O<sub>2</sub>/C<sub>3</sub>H<sub>8</sub> ratio than that of acetate species, and more than double from ~35 per-Pt-site with O<sub>2</sub>/C<sub>3</sub>H<sub>8</sub> equal to 5, to ~75 per-Pt-site with O<sub>2</sub>/C<sub>3</sub>H<sub>8</sub> equal to 20. These results are consistent with the DRIFTS spectra (Section S.7 in the Supporting Information) showing that the intensity of the bands associated with enolate, aliphatic ester, and acetone increases when increasing the O<sub>2</sub>/C<sub>3</sub>H<sub>8</sub> ratio from 5 to 20. As the initial concentration of EEA species increases, the temperature of the maximum CO<sub>2</sub> evolution rate from combustion of EEA species decreases from ~460 °C to ~430 °C, which is characteristic of 2nd-order surface reaction kinetics. Therefore, the maximum CO<sub>2</sub> evolution rate during TPO occurs at a lower temperature with O<sub>2</sub>/C<sub>3</sub>H<sub>8</sub> equal to 20 (Fig. 3(b)) than that with O<sub>2</sub>/C<sub>3</sub>H<sub>8</sub> equal to 5 (Fig. 3(a)), because there is a higher concentration of the more reactive EEA species with O<sub>2</sub>/C<sub>3</sub>H<sub>8</sub> equal to 20.

### 3.3. The role of oxy-carbon surface species in the propane oxidation mechanism

The oxy-carbon species formed on the surface of Pt/Al<sub>2</sub>O<sub>3</sub> during propane oxidation can be classified, according to their role in the propane oxidation mechanism, as (1) reactive intermediates which lead directly to CO<sub>2</sub> formation, (2) poisoning species which block the active sites for CO<sub>2</sub> formation, or (3) spectator species which do not contribute significantly to the observed CO<sub>2</sub> formation. To determine the role of oxy-carbon surface species in the mechanism of propane total oxidation to CO<sub>2</sub>, the rate of CO<sub>2</sub> production in the gas-phase was measured by micro GC analysis of the product gas while the concentration of oxy-carbon species on the surface of the catalyst was measured by DRIFTS simultaneously.

Fig. 5 shows the CO<sub>2</sub> production rate, and Fig. 1(c) shows the concentration of oxy-carbon surface species, during propane oxidation over Pt/Al<sub>2</sub>O<sub>3</sub> at 300 °C with O<sub>2</sub>/C<sub>3</sub>H<sub>8</sub> equal to 20. The CO<sub>2</sub> production rates in Fig. 5 have been published previously, and a more detailed analysis of the kinetics of the reaction is given in that publication [2]. While the CO<sub>2</sub> production rate in Fig. 5 is nearly constant at ~0.8 s<sup>-1</sup> over the entire 400 min of the reaction,

the concentration of oxy-carbon surface species in Fig. 1(c) increases continuously until a steady-state is reached after ~200 min of the reaction. In general, there is no correlation between the concentration of oxy-carbon surface species and the rate of CO<sub>2</sub> production in the gas-phase for all six reaction conditions (see Section S.8 in the Supporting Information), which indicates that the growth of oxy-carbon surface species does not influence the CO<sub>2</sub> production rate and these species are inert spectators in the propane oxidation mechanism.

Fig. 5 also shows the rate of carbon accumulation on the Al<sub>2</sub>O<sub>3</sub> support, which was calculated by taking the time-derivative of the total amount of surface carbon from Fig. 1(c) and normalizing to the number of surface Pt sites (see Eq. (S10) in the Supporting Information). The rate of carbon accumulation is ~0.1 s<sup>-1</sup> at the beginning of the reaction and decreases to ~0.01 s<sup>-1</sup> during the first 100 min of the reaction. Similar results were obtained for all six reaction conditions (see Section S.9 in the Supporting Information), and the rate of surface carbon accumulation is ~1-to-3 orders-of-magnitude lower than the CO<sub>2</sub> production rate for all reaction conditions.

The rates of CO<sub>2</sub> production from combustion of the acetate and EEA species were calculated using Eqs. (1) and (2), respectively, and assuming concentrations of acetate (27 per-Pt-site) and EEA (75 per-Pt-site) species. These concentrations were taken from the areas of the modeled acetate and EEA TPO curves in Fig. 4(b) and represent their steady-state concentrations at 300 °C with O<sub>2</sub>/C<sub>3</sub>H<sub>8</sub> equal to 20. The rate of CO<sub>2</sub> production from combustion of acetate at 300 °C is ~5 · 10<sup>-5</sup> s<sup>-1</sup>, which is about 4 orders-of-magnitude lower than the experimentally observed CO<sub>2</sub> production rate of 0.8 s<sup>-1</sup>. The rate of CO<sub>2</sub> production from combustion of the higher reactivity EEA species is ~0.01 s<sup>-1</sup> at 300 °C, which is nearly 2 orders-of-magnitude lower than the observed CO<sub>2</sub> production rate. These results clearly indicate that the growth of oxy-carbon surface species, and their combustion to CO<sub>2</sub>, occurs via reaction pathways that are parallel to, and several orders-of-magnitude slower than, the main pathway to CO<sub>2</sub> production.

#### 3.4. Mechanism of oxy-carbon surface species growth

While it is beyond the scope of this work to discuss the detailed mechanism of oxy-carbon surface species growth, which likely

involves several parallel pathways and hundreds of possible elementary steps, we can speculate about several aspects of their growth. The growth of oxy-carbon surface species on the Al<sub>2</sub>O<sub>3</sub> support without dispersed platinum nanoparticles is negligible (see Section S.12 in the Supporting Information). This indicates that platinum nanoparticles catalyze the transformation of propane and oxygen into oxy-carbon surface species, which spill over and grow on the Al<sub>2</sub>O<sub>3</sub> support. The growth rate of these oxy-carbon surface species is ~1-to-3 orders-of-magnitude slower than the observed CO<sub>2</sub> production rate, which may suggest that platinum sites at the interface between the Al<sub>2</sub>O<sub>3</sub> support and the platinum nanoparticles, which comprise only a small fraction of the total surface platinum atoms, are the active sites for oxy-carbon surface species growth whereas the platinum atoms further from the Pt/Al<sub>2</sub>O<sub>3</sub> interface are the active sites for the main pathway to CO<sub>2</sub> production.

Following their activation at Pt/Al<sub>2</sub>O<sub>3</sub> interfacial sites, the oxy-carbon surface species then grow radially from the platinum nanoparticles on the Al<sub>2</sub>O<sub>3</sub> support. These oxy-carbon surface species must diffuse outwardly, or react to form CO<sub>2</sub> at the Pt/Al<sub>2</sub>O<sub>3</sub> interface, to create open sites for spillover from the platinum nanoparticles. As the coverage of oxy-carbon surface species increases, the rate of carbon accumulation decreases until their concentration reaches a steady-state. The steady-state concentration is dependent on the reaction conditions (see Fig. S5 in the Supporting Information), and therefore, the steady-state carbon concentration does not represent a saturation coverage but rather an equilibrium coverage in which the rate of oxy-carbon species growth is roughly equal to their rate of combustion.

While the concentration of acetate species is relatively insensitive to the reaction conditions, the concentration of the higher reactivity EEA species generally increases with increasing O<sub>2</sub>/C<sub>3</sub>H<sub>8</sub> ratio and decreasing temperature (Fig. 3 and Fig. S6 in the Supporting Information). Higher O<sub>2</sub>/C<sub>3</sub>H<sub>8</sub> ratios and lower temperatures are also conditions which generally lead to higher oxygen coverages on the platinum nanoparticles and platinum-oxide formation [2]. This may suggest that high oxygen coverages may increase the rate of EEA growth, or decrease the rate of EEA combustion, or both. Future work will focus on the formation of the EEA species near the Pt/Al<sub>2</sub>O<sub>3</sub> interface, and the influence of oxygen coverage on their formation. The support also plays an important role in the growth of oxy-carbon surface species and a detailed investigation of the influence of the support on the growth of oxy-carbon surface species would yield valuable insights into the mechanisms of oxy-carbon surface species growth.

#### 4. Conclusions

The growth of oxy-carbon species on the surface of Pt/Al<sub>2</sub>O<sub>3</sub> during propane oxidation was investigated in detail by DRIFTS to clarify their role in the propane oxidation mechanism. We showed that there are many different oxy-carbon species that grow on the surface of Pt/Al<sub>2</sub>O<sub>3</sub> during propane oxidation. Platinum nanoparticles catalyze the formation of these species, which then spill over and grow on the Al<sub>2</sub>O<sub>3</sub> support. Temperature-programmed oxidation of the oxy-carbon surface species indicates that there are two main types of oxy-carbon surface species: lower reactivity acetate species and higher reactivity EEA species. There is no correlation between the concentration of oxy-carbon surface species and the rate of CO<sub>2</sub> production in the gas-phase, and therefore, these species are inert spectators in the propane oxidation mechanism. Both the rate of oxy-carbon accumulation on the Al<sub>2</sub>O<sub>3</sub> support, and the rate of combustion of the oxy-carbon surface species, are several orders-of-magnitude lower than the rate of CO<sub>2</sub> production in the gas-phase.

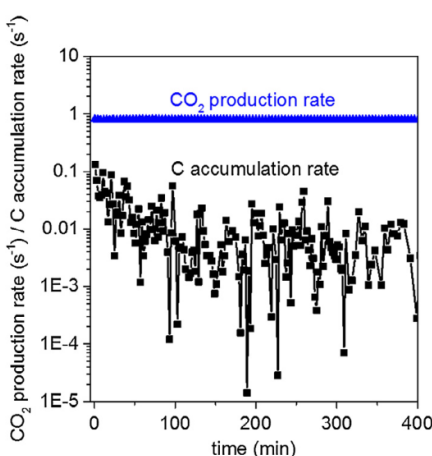


**Fig. 5.** Comparison of the CO<sub>2</sub> production rate in the gas-phase (blue data points) to the rate of carbon deposition on the Al<sub>2</sub>O<sub>3</sub> surface (black data points) during propane oxidation over Pt/Al<sub>2</sub>O<sub>3</sub> with O<sub>2</sub>/C<sub>3</sub>H<sub>8</sub> equal to 20 and at 300 °C. The CO<sub>2</sub> production rates have been published previously [2].

## Acknowledgments

Research was sponsored by the U.S. Army Research Laboratory and was accomplished under Cooperative Agreement Number W911NF-12-2-0019. The views and conclusions contained in this document are those of the authors and should not be interpreted as representing the official policies, either expressed or implied, of the U.S. Army Research Laboratory or the U.S. Government. The U.S. Government is authorized to reproduce and distribute reprints for Government purposes notwithstanding any copyright notation herein.

## Appendix A. Supplementary material

Supplementary data associated with this article can be found, in the online version, at <http://dx.doi.org/10.1016/j.jcat.2016.12.021>.

## References

- [1] D.L. Trimm, Catalytic combustion (review), *Appl. Catal. A* 7 (1983) 249–282.
- [2] C.P. O'Brien, G.R. Jenness, H. Dong, D.G. Vlachos, I.C. Lee, Deactivation of Pt/Al<sub>2</sub>O<sub>3</sub> during propane oxidation at low temperatures: kinetic regimes and platinum oxide formation, *J. Catal.* 337 (2016) 122–132.
- [3] P. Forzatti, L. Liotti, Catalyst deactivation, *Catal. Today* 52 (1999) 165–181.
- [4] C.H. Bartholomew, Mechanisms of catalyst deactivation, *Appl. Catal. A-Gen.* 212 (2001) 17–60.
- [5] W.I.S. Faria, C.A.C. Perez, D.V. Cesar, L.C. Dieguez, M. Schmal, In situ characterizations of Pd/Al<sub>2</sub>O<sub>3</sub> and Pd/CeO<sub>2</sub>/Al<sub>2</sub>O<sub>3</sub> catalysts for oxidative steam reforming of propane, *Appl. Catal. B-Environ.* 92 (2009) 217–224.
- [6] A. Hinz, M. Skoglundh, E. Fredell, A. Andersson, An investigation of the reaction mechanism for the promotion of propane oxidation over Pt/Al<sub>2</sub>O<sub>3</sub> by SO<sub>2</sub>, *J. Catal.* 201 (2001) 247–257.
- [7] P.A. Carlsson, S. Möller, K. Arnby, M. Skoglundh, Effect of periodic operation on the low-temperature activity for propane oxidation over Pt/Al<sub>2</sub>O<sub>3</sub> catalysts, *Chem. Eng. Sci.* 59 (2004) 4313–4323.
- [8] X.D. Wu, L. Zhang, D. Weng, S. Liu, Z.C. Si, J. Fan, Total oxidation of propane on Pt/WO<sub>x</sub>/Al<sub>2</sub>O<sub>3</sub> catalysts by formation of metastable Pt delta+ species interacted with WO<sub>x</sub> clusters, *J. Hazard. Mater.* 225 (2012) 146–154.
- [9] E. Finocchio, G. Busca, V. Lorenzelli, R.J. Willey, The activation of hydrocarbon C–H bonds over transition-metal oxide catalysts – a FTIR study of hydrocarbon catalytic combustion over MgCr<sub>2</sub>O<sub>4</sub>, *J. Catal.* 151 (1995) 204–215.
- [10] E. Finocchio, R.J. Willey, G. Busca, V. Lorenzelli, FTIR studies on the selective oxidation and combustion of light hydrocarbons at metal oxide surfaces. 3. Comparison of the oxidation of C-3 organic compounds over Co<sub>3</sub>O<sub>4</sub>, MgCr<sub>2</sub>O<sub>4</sub> and CuO, *J. Chem. Soc.-Faraday Trans. 93* (1997) 175–180.
- [11] B. Wang, X.D. Wu, R. Ran, Z.C. Si, D. Weng, IR characterization of propane oxidation on Pt/CeO<sub>2</sub>-ZrO<sub>2</sub>: the reaction mechanism and the role of Pt, *J. Mol. Catal. A-Chem.* 356 (2012) 100–105.
- [12] Z.D. Yigezu, K. Muthukumar, Structural characteristics of selected metal oxides used for the catalytic pyrolysis of sunflower oil, *J. Anal. Appl. Pyrol.* 114 (2015) 60–67.
- [13] R. Anbarasan, V. Dhanalakshmi, Melt functionalization of LDPE with thio ester, amino ester, and hydroxy ester by thermolysis method—an FTIR study, *J. Appl. Polym. Sci.* 122 (2011) 2252–2261.
- [14] J. van den Brand, O. Blajiev, P.C.J. Beentjes, H. Terryn, J.H.W. de Wit, Interaction of ester functional groups with aluminum oxide surfaces studied using infrared reflection absorption spectroscopy, *Langmuir* 20 (2004) 6318–6326.
- [15] S.M.K. Airaksinen, M.A. Banares, A.O.I. Krause, In situ characterisation of carbon-containing species formed on chromia/alumina during propane dehydrogenation, *J. Catal.* 230 (2005) 507–513.
- [16] M.I. Zaki, M.A. Hasan, F.A. Al-Sagheer, L. Pasupulety, Surface chemistry of acetone on metal oxides: IR observation of acetone adsorption and consequent surface reactions on silica-alumina versus silica and alumina, *Langmuir* 16 (2000) 430–436.
- [17] H. Deng, Y.B. Yu, H. He, Discerning the role of Ag-O-Al entities on Ag/gamma-Al<sub>2</sub>O<sub>3</sub> surface in NO<sub>x</sub> selective reduction by ethanol, *J. Phys. Chem. C* 119 (2015) 3132–3142.
- [18] D.G. Rethwisch, J.A. Dumesic, Effect of metal oxygen bond strength on properties of oxides 1. Infrared-spectroscopy of adsorbed CO and CO<sub>2</sub>, *Langmuir* 2 (1986) 73–79.
- [19] M.M. Schubert, H.A. Gasteiger, R.J. Behm, Surface formates as side products in the selective CO oxidation on Pt/gamma-Al<sub>2</sub>O<sub>3</sub>, *J. Catal.* 172 (1997) 256–258.
- [20] V. Ermini, E. Finocchio, S. Sechi, G. Busca, S. Rossini, An FT-IR and flow reactor study of the conversion of propane on gamma-Al<sub>2</sub>O<sub>3</sub> in oxygen-containing atmosphere, *Appl. Catal. A-Gen.* 190 (2000) 157–167.
- [21] H.A. Al-Abadleh, V.H. Grassian, FT-IR study of water adsorption on aluminum oxide surfaces, *Langmuir* 19 (2003) 341–347.
- [22] S. Guerrero, J.T. Miller, A.J. Kropf, E.E. Wolf, In situ EXAFS and FTIR studies of the promotion behavior of Pt-Nb<sub>2</sub>O<sub>5</sub>/Al<sub>2</sub>O<sub>3</sub> catalysts during the preferential oxidation of CO, *J. Catal.* 262 (2009) 102–110.
- [23] J. Baltrusaitis, J.H. Jensen, V.H. Grassian, FTIR spectroscopy combined with isotope labeling and quantum chemical calculations to investigate adsorbed bicarbonate formation following reaction of carbon dioxide with surface hydroxyl groups on Fe<sub>2</sub>O<sub>3</sub> and Al<sub>2</sub>O<sub>3</sub>, *J. Phys. Chem. B* 110 (2006) 12005–12016.
- [24] C. Morterra, G. Magnacca, A case study: surface chemistry and surface structure of catalytic aluminas, as studied by vibrational spectroscopy of adsorbed species, *Catal. Today* 27 (1996) 497–532.
- [25] J. Wan, R. Ran, M. Li, X. Wu, D. Weng, Effect of acid and base modification on the catalytic activity of Pt/Al<sub>2</sub>O<sub>3</sub> for propene oxidation, *J. Mol. Catal. A-Chem.* 383 (2014) 194–202.
- [26] Y.B. Yu, H. He, Q.C. Feng, Novel enolit surface species formed during partial oxidation of CH<sub>3</sub>CHO, C<sub>2</sub>H<sub>5</sub>OH, and C<sub>3</sub>H<sub>8</sub> on Ag/Al<sub>2</sub>O<sub>3</sub>: an in situ DRIFTS study, *J. Phys. Chem. B* 107 (2003) 13090–13092.
- [27] Y. Yan, Y. Yu, H. He, J. Zhao, Intimate contact of enolic species with silver sites benefits the SCR of NO<sub>x</sub> by ethanol over Ag/Al<sub>2</sub>O<sub>3</sub>, *J. Catal.* 293 (2012) 13–26.
- [28] H.W. Gao, H. He, Y.B. Yu, T.X. Yan, DFT and experimental investigations of the formation and adsorption of enolic species on Al<sub>2</sub>O<sub>3</sub> catalyst, *J. Mol. Struct.* 892 (2008) 320–324.
- [29] P.S. Kim, M.K. Kim, B.K. Cho, I.S. Nam, Autocatalytic synergism observed during lean-NO<sub>x</sub> reduction with a bifunctional reductant over Ag/Al<sub>2</sub>O<sub>3</sub> catalyst, *J. Catal.* 292 (2012) 44–52.
- [30] Y.B. Yu, H. He, Q.C. Feng, H.W. Gao, X. Yang, Mechanism of the selective catalytic reduction of NO<sub>x</sub> by C<sub>2</sub>H<sub>5</sub>OH over Ag/Al<sub>2</sub>O<sub>3</sub>, *Appl. Catal. B-Environ.* 49 (2004) 159–171.
- [31] Y.B. Yu, J.J. Zhao, Y. Yan, X. Han, H. He, A cyclic reaction pathway triggered by ammonia for the selective catalytic reduction of NO<sub>x</sub> by ethanol over Ag/Al<sub>2</sub>O<sub>3</sub>, *Appl. Catal. B-Environ.* 136 (2013) 103–111.
- [32] Y. Yu, X. Song, H. He, Remarkable influence of reductant structure on the activity of alumina-supported silver catalyst for the selective catalytic reduction of NO<sub>x</sub>, *J. Catal.* 271 (2010) 343–350.
- [33] H. He, Y.B. Yu, Selective catalytic reduction of NO<sub>x</sub> over Ag/Al<sub>2</sub>O<sub>3</sub> catalyst: from reaction mechanism to diesel engine test, *Catal. Today* 100 (2005) 37–47.
- [34] Y. Yu, H. He, X. Zhang, H. Deng, A common feature of H<sub>2</sub>-assisted H-SCR over Ag/Al<sub>2</sub>O<sub>3</sub>, *Catal. Sci. Technol.* 4 (2014) 1239–1245.
- [35] H.W. Gao, T.X. Yan, Y.B. Yu, H. He, DFT and DRIFTS studies on the adsorption of acetate on the Ag/Al<sub>2</sub>O<sub>3</sub> catalyst, *J. Phys. Chem. C* 112 (2008) 6933–6938.
- [36] M. Cruz, R.M. Sanchez-Sánchez, Navarro Yerga, D.I. Kondarides, X.E. Verykios, J. L.G. Fierro, Mechanistic aspects of the ethanol steam reforming reaction for hydrogen production on Pt, Ni, and PtNi catalysts supported on gamma-Al<sub>2</sub>O<sub>3</sub>, *J. Phys. Chem. A* 114 (2010) 3873–3882.
- [37] M. Domok, A. Oszko, K. Baan, I. Sarusi, A. Erdohelyi, Reforming of ethanol on Pt/Al<sub>2</sub>O<sub>3</sub>-ZrO<sub>2</sub> catalyst, *Appl. Catal. A-Gen.* 383 (2010) 33–42.
- [38] D.K. Captain, M.D. Amiridis, In situ FTIR studies of the selective catalytic reduction of NO by C<sub>2</sub>H<sub>6</sub> over Pt/Al<sub>2</sub>O<sub>3</sub>, *J. Catal.* 184 (1999) 377–389.
- [39] M. Haneda, N. Bion, M. Daturi, J. Saussey, J.C. Lavalle, D. Duprez, H. Hamada, In situ Fourier transform infrared study of the selective reduction of NO with propane over Ga<sub>2</sub>O<sub>3</sub>-Al<sub>2</sub>O<sub>3</sub>, *J. Catal.* 206 (2002) 114–124.
- [40] K. Shimizu, H. Kawabata, A. Satsuma, T. Hattori, Role of acetate and nitrates in the selective catalytic reduction of NO by propane over alumina catalyst as investigated by FTIR, *J. Phys. Chem. B* 103 (1999) 5240–5245.
- [41] V. Matsouka, M. Konsolakis, R.M. Lambert, I.V. Yentekakis, In situ DRIFTS study of the effect of structure (CeO<sub>2</sub>-La<sub>2</sub>O<sub>3</sub>) and surface (Na) modifiers on the catalytic and surface behaviour of Pt/gamma-Al<sub>2</sub>O<sub>3</sub> catalyst under simulated exhaust conditions, *Appl. Catal. B-Environ.* 84 (2008) 715–722.
- [42] M. Kakihana, M. Akiyama, Vibrational analysis of the propionate ion and its C-13 derivatives - infrared low-temperature spectra, normal-coordinate analysis, and local-symmetry valence force-field, *J. Phys. Chem.* 91 (1987) 4701–4709.
- [43] S.R. Tong, L.Y. Wu, M.F. Ge, W.G. Wang, Z.F. Pu, Heterogeneous chemistry of monocarboxylic acids on alpha-Al<sub>2</sub>O<sub>3</sub> at different relative humidities, *Atmos. Chem. Phys.* 10 (2010) 7561–7574.
- [44] A.R. McInroy, D.T. Lundie, J.M. Winfield, C.C. Dudman, P. Jones, D. Lennon, The application of diffuse reflectance infrared spectroscopy and temperature-programmed desorption to investigate the interaction of methanol on eta-alumina, *Langmuir* 21 (2005) 11092–11098.
- [45] D.N. Goldstein, J.A. McCormick, S.M. George, Al<sub>2</sub>O<sub>3</sub> atomic layer deposition with trimethylaluminum and ozone studied by in situ transmission FTIR spectroscopy and quadrupole mass spectrometry, *J. Phys. Chem. C* 112 (2008) 19530–19539.
- [46] J.H. Kwon, M. Dai, M.D. Halls, Y.J. Chabal, Detection of a formate surface intermediate in the atomic layer deposition of high-k dielectrics using ozone, *Chem. Mater.* 20 (2008) 3248–3250.
- [47] E. Ozensoy, D. Herling, J. Szanyi, NO<sub>x</sub> reduction on a transition metal-free gamma-Al<sub>2</sub>O<sub>3</sub> catalyst using dimethylether (DME), *Catal. Today* 136 (2008) 46–54.
- [48] X.S. Liu, R.E. Pruitt, DRFT-IR studies of the surface of gamma-alumina, *J. Am. Chem. Soc.* 119 (1997) 9856–9860.
- [49] E. Heracleous, A.A. Lemonidou, J.A. Lercher, Mechanistic features of the ethane oxidative dehydrogenation by in situ FTIR spectroscopy over a MoO<sub>3</sub>/Al<sub>2</sub>O<sub>3</sub> catalyst, *Appl. Catal. A-Gen.* 264 (2004) 73–80.
- [50] H. Knozinger, P. Ratnasamy, Catalytic aluminas - surface models and characterization of surface sites, *Catal. Rev.-Sci. Eng.* 17 (1978) 31–70.
- [51] C.A. Querini, S.C. Fung, Temperature-programmed oxidation technique: kinetics of coke-O<sub>2</sub> reaction on supported metal catalysts, *Appl. Catal. A* 117 (1994) 53–74.

- [52] F. Larachi, K. Belkacemi, S. Hamoudi, A. Sayari, Kinetics of carbon oxide evolution in temperature-programmed oxidation of carbonaceous laydown deposited on wet oxidation catalysts, *Catal. Today* 64 (2001) 163–177.
- [53] M.A. Peralta, M.S. Gross, B.S. Sánchez, C.A. Querini, Catalytic combustion of diesel soot: experimental design for laboratory testing, *Chem. Eng. J.* 152 (2009) 234–241.
- [54] B. Sánchez, M.S. Gross, B.D. Costa, C.A. Querini, Coke analysis by temperature-programmed oxidation: morphology characterization, *Appl. Catal. A* 364 (2009) 35–41.
- [55] C. Kern, A. Jess, Regeneration of coked catalysts—modelling and verification of coke burn-off in single particles and fixed bed reactors, *Chem. Eng. Sci.* 60 (2005) 4249–4264.
- [56] S. Mahamulkar, K. Yin, P.K. Agrawal, R.J. Davis, C.W. Jones, A. Malek, H. Shibata, Formation and oxidation/gasification of carbonaceous deposits: a review, *Ind. Eng. Chem. Res.* 55 (2016) 9760–9818.

